*American Mineralogist, Volume 93, pages 584–590, 2008*

# Structure and reactivity of synthetic Co-substituted goethites

**Mariana Alvarez,[1,*] Elsa E. Sileo,[2] and Elsa H. Rueda[1]**

[1]Departamento de Química, Universidad Nacional del Sur, Avenida Alem 1253, B8000CPB, Bahía Blanca, Argentina
[2]INQUIMAE, Departamento de Química Inorgánica, Analítica y Química Física, Facultad de Ciencias Exactas y Naturales, Universidad de Buenos Aires, Argentina

## Abstract

A set of synthetic goethites were prepared from $Fe^{3+}$- and $Co^{2+}$-nitrate solutions in alkaline media with a Co/(Co + Fe) ratio ($x_{Co}$) up to 10 mol%. The structural characterization of the resultant solid phases was carried out by X-ray diffraction (XRD). XRD analyses showed that in preparations with $x_{Co}$ <10 mol%, Co-substituted goethite was the only crystalline phase present. Atomic and cell parameters for the samples synthesized were obtained by the Rietveld refinement of the XRD data, and showed that the unit cell in the goethite-like phase is contracted as a function of $x_{Co}$. Little deviation from the Vegard rule was observed for all unit-cell parameters. Cobalt substitution produces an increase in the surface area of the goethite, as well as an increment in the dehydroxylation temperature. The acid dissolution of all Co-goethites showed an increase in dissolution rate with the Co content, and a congruent behavior was observed. The activation energy for dissolution was obtained two samples. A modified first-order Kabai equation best describes the dissolution data.

**Keywords:** Co-goethite, isomorphous substitution, Rietveld refinement, acid dissolution

## Introduction

Goethite is the most common Fe oxide present in soils (Cornell and Schwertmann 1996). Goethite has isostructural equivalents in which cations, other than Fe, occupy the interstices of the oxygen framework. Most of these oxide-hydroxides exist as pure minerals although they are rarer than goethite. The existence of these structural compounds suggests the likelihood of isomorphous substitution for $Fe^{3+}$ by other cations. Naturally occurring goethite is unlikely to exist in pure form, and different foreign elements such as Al, Mn, Cr, and Ni may be present in its structure (Kühnel et al. 1975; Norrish 1975; Schwertmann and Taylor 1989). Isomorphous replacement of Fe in the goethite structure by other cations can be readily achieved in synthetic goethites.

The incorporation of foreign ions alter the properties of goethite such as its cell parameters, structural OH content, thermal and magnetic properties, and dissolution behavior (Murad and Schwertmann 1983; Schwertmann 1984; Gasser et al. 1996; Pozas et al. 2004). Among the foreign cations, Co is attractive because of its significance for plant and animal nutrition (Alloway 1990). Besides, Co-substituted goethite has been used as precursor for the production of Co-Fe metallic particles (Iwasaki and Yamamura 2002; Nuñez et al. 2003).

Different aspects of Co-substituted goethite obtained in alkaline media have been studied by other authors (Cornell and Giovanoli 1989; Gerth 1990; Cornell 1991; Gasser et al. 1996; Iwasaki and Yamamura 2002). Recent studies of Co-goethites obtained from aerial oxidation of both $Fe^{2+}$ and $Co^{2+}$ solutions were carried out by Pozas et al. (2002, 2004).

The aim of this work was to obtain Co-substituted goethite by co-precipitation of $Fe^{3+}$ and $Co^{2+}$ solutions in alkaline media by the same pathway described for the synthesis of Mn-substituted goethite (Sileo et al. 2001). Then, the morphology, thermal, and acid dissolution behavior of these samples was studied as a function of Co content in the goethite structure. The unit-cell parameters and atomic distances were calculated by the Rietveld refinement method (Rietveld 1969).

## Experimental methods

### Materials

The α-FeOOH particles were prepared from mixed ferrihydrites containing different molar ratios ($x_{Co}$) that varied in the 0–10 mol% percent range. Ferrihydrites were precipitated by adding 2 mol/dm$^3$ NaOH solution to different $Fe^{3+}$ and $Co^{2+}$ nitrate solutions; final ratio $Me/OH^-$ in all preparations was 0.076. Initial Fe + Co concentration was 0.53 mol/dm$^3$ in all samples. The resultant precipitates were washed twice with doubly distilled water and centrifuged. After this treatment, the samples were held at 60 °C for 15 days in closed polyethylene flasks containing 0.3 mol/dm$^3$ NaOH. Initial values of (Co)/(Co + Fe) × 100 mole ratios ($x_{Co}$) were 0, 3, 5, 7, and 10 mol% (samples were named $G_0$, $G_3$, $G_5$, $G_7$, and $G_{10}$, respectively). After the aging period, the samples were centrifuged, dried at 40 °C, and the amorphous materials were extracted with 0.4 mol/dm$^3$ HCl at room temperature (Cornell and Giovanoli 1989). The crystalline solids were washed with doubly distilled water until the conductivity of the filtrated solution was similar to that of doubly distilled water. The final samples were dried at 40 °C and gently crushed. All chemicals used were reagent grade.

### Characterization

The Fe and Co contents were determined by atomic absorption spectrometry (AAS) in a GBC, Model B-932 spectrometer. Chemical analyses were made in duplicate by dissolving the samples in concentrated HCl and diluting to an adequate concentration with water. Diffraction patterns were recorded using a Siemens D5000 diffractometer in a Bragg-Brentano geometry equipped with Cu$K\alpha$ radiation and a graphite monochromator. Data were collected in the $18.500° \le 2\theta \le 132.000°$ range; the scanning step was 0.025°. Divergence, scattered, and receiving radiation slits were 1°, 1°, and 0.2 mm, respectively. The step width assured a minimum of about 12 intensity points for the narrower peaks. Generator settings were fixed at

* E-mail: alvarezm@criba.edu.ar

40 kV and 35 mA. The data were analyzed using the GSAS (Larson and Von Dreele 2004) system. Starting unit-cell parameters and atomic coordinates for goethite were taken from the literature (Szytula et al. 1968). Peak profiles were fitted using the Thompson-Cox-Hastings pseudo-Voigt function (Thompson et al. 1987) with the microstrain broadening description of Stephens (1999). Peak asymmetry was corrected using the Finger function (Finger et al. 1994).

As the XRD diagram showed that peaks corresponding to the family of diffracting planes (021) were sharper than others, the [021] axis, perpendicular to planes (021) was used as the anisotropy axis. The coherent scattering domains or crystallite size dimensions were then obtained adopting the anisotropic bidimensional model described in the GSAS manual. The anisotropic dimensions of the crystallites were determined over the entire diffraction pattern in the parallel ($p_{paral}$) and perpendicular direction ($p_{perp}$) to the anisotropic broadening [021] axis. The dimensions of the scattering domains were calculated taking into account the instrument broadening function that was defined using NIST SRM 660 lanthanum hexaboride ($LaB_6$) standard. Only the Lorentzian component of the peak file function was used to calculate $p_{perp}$ and $p_{paral}$.

Specimens for scanning electron microscopy (SEM) were dispersed in double-distilled water with ultrasonic treatment and a drop of suspension was placed onto a conductive carbon tape support. SEM images were obtained from a Field Emission Gun (FEG) Zeiss DSM 982 GEMINI equipment operated at 5 kV. Processing and analyses of the SEM images was carried out with the Analysis Pro 3.11 software, and between 60 and 85 particles were measured for each sample.

The surface area (SA) was measured by $N_2$-adsorption at 77 K in the range $P/P_0$ 0.05–0.3 by means of a Quantachrome NOVA 1200e.

Thermogravimetry-differential thermal analysis (TG-DTA) curves were obtained in air at a heating rate of 10 °C/min on a Rigaku Thermoflex TG 8110 instrument, attached to a Therma Analysis Station TAS 100.

### Reactivity

Dissolution kinetics were measured at temperatures from 40 to 60 °C. Fifty milligrams of each sample was suspended in 50 $cm^3$ of 4 $mol/dm^3$ HCl and sealed in a glass baker provided with a thermostat water jacket. The suspension was magnetically stirred throughout the experiment. Suspension aliquots (1 $cm^3$) were withdrawn at predetermined intervals and filtered through 0.22 μm membrane filters. The solution to solid weight ratio (1000:1) used in this work is in line with previous dissolution studies that used ratios in the range 250–2000:1 to ensure that the dissolution was independent of this ratio (Cornell et al. 1974; Sidhu et al. 1981; Lim-Nuñez and Gilkes 1987). Dissolved Fe and Co amounts were determined by AAS.

To determine activation energy ($E_a$), dissolution kinetics were measured at three temperatures (40, 50, and 60 °C). All kinetic experiments were carried out in duplicate and the coefficient of variation was <0.08.

## Results and discussion

The Co and Fe content of the particles produced at different values of $x_{Co}$ are presented in Table 1. Although previous studies reported lesser amounts of Co incorporated into goethite, the measured $x_{Co}$ values in Table 1 confirm that the synthesis procedure used in this work renders samples with $x_{Co}$ close to those in the starting solutions. The data also reveal that the Co ions are readily incorporated into the goethite particles.

Samples contained up to 9.9 ± 0.2 mol% Co. The surface area increases as $x_{Co}$ increases (Table 1). A linear relationship between SA and Co content was found for samples $G_0$ to $G_7$ ($R^2$ = 0.999; $n$ = 4). The linearity is lost at $G_{10;}$ this behavior could be associated with a large increase in SA (102.6 $m^2/g$). This increase will be discussed below, together with the XRD data and SEM images.

**Table 1.** Composition and surface area of Co-substituted goethite samples

| Samples | $x_{Co\ (nominal)}$ mol% | $x_{Co\ (experimental)}$ mol% | Surface area ($m^2/g$) | $H_2O$% (stoichiometric) |
|---|---|---|---|---|
| $G_0$ | 0.0 | 0.0 | 38.9 | n.d. |
| $G_3$ | 3.0 | 3.1 ± 0.2 | 49.2 | 12.23 (10.12) |
| $G_5$ | 5.0 | 4.1 ± 0.1 | 51.5 | 11.99 (10.11) |
| $G_7$ | 7.0 | 6.7 ± 0.1 | 59.8 | 12.28 (10.11) |
| $G_{10}$ | 10.0 | 9.9 ± 0.2 | 102.6 | 11.20 (10.09) |

*Note:* n.d. = not determined.

Similar studies concerning Mn-substituted goethites (Sun et al. 1999) have demonstrated that the BET area of Mn-goethites with similar degrees of substitution varies in the range 40–37.3 $m^2/g$, indicating a quite different effect of both cations Co and Mn on the surface of goethite.

Figure 1 shows the scanning electron micrographs of the acicular particles in the series. The average length, as measured by SEM, increases from $G_3$ to $G_7$ and thus with an increase in $x_{Co}$. Sample $G_{10}$ displays a higher polydispersion, and an incipient unknown phase with spherical morphology was detected.

The particle size distribution of samples $G_3$ to $G_7$ is presented in Figure 2; average particle sizes are 215 nm for $G_3$, 376 nm for $G_5$, and 450 nm for $G_7$.

With the aim of showing the changes in the aggregation of needles with an increase in $x_{Co,}$ an additional comparison between $G_0$ and $G_{10}$, at a higher magnification (100 000×), is presented in Figure 3. As can be seen, the degree of aggregation decreases from $G_0$ to $G_{10}$, and this could be an additional effect of the increase in surface area, besides the appearance of a new incipient phase.

Table 1 also shows the water content up to 500 °C, measured by the mass loss in TGA experiments according to the following equation:

$$\alpha\text{-}(Fe_{1-x}Co_x)_{1-y/3}O_{1-y}(OH)_{1+y} \rightarrow (1-y/3)\ \alpha\text{-}(Fe_{1-x}Co_x)_2O_3 + (1+y)\ H_2O.$$

Heating in the temperature range from 30 to 140 °C eliminates adsorbed water. According to TGA measurements, the content does not exceed 1 wt% in all samples. Structural water, which defines the $OH^-/O^{2-}$ ratio, is eliminated in the range from 140–500 °C. In samples $G_0$ to $G_{10}$, this ratio exceeds the value of 1, typical of stoichiometric goethite ($H_2O$ wt% = 10.13), which is indicative of metal deficient goethites. Similar features were observed in Al- and Cr-substituted goethites (Wolska and Schwertmann 1989; Sileo et al. 2004).

Figure 4 shows the DTA traces. The endothermic peak corresponding to the structural water released from the $OH^-$ groups is displaced to higher temperatures when the Co content increases. The same feature was observed for Al- and Mn-substituted goethites (Schulze and Schwertmann 1984; Alvarez et al. 2006).

The release of $OH^-$ groups of sample $G_3$ shows a peak centered at 268 °C ($T_\beta$) and a shoulder at 245 °C ($T_\alpha$) that splits into two peaks ($T_\alpha$ and $T'_\alpha$) when $x_{Co}$ increases. Heterogeneity in particle size as shown in SEM images, as well as lattice distortions and defects have been cited as the cause of the multiple peaks (Ishikawa et al. 2000).

XRD patterns for samples $G_3$ to $G_7$ only showed a goethite-like structure. Sample $G_{10}$ showed additional low-intensity peaks attributable to a separate phase (see Fig. 5). This new phase (probably magnetite or maghemite) could not be properly identified by XRD because of the small amount and the nanometric size of the particles.

To confirm the Fe-for-Co substitution in the series, we calculated the unit-cell parameters for pure goethite and all Co-

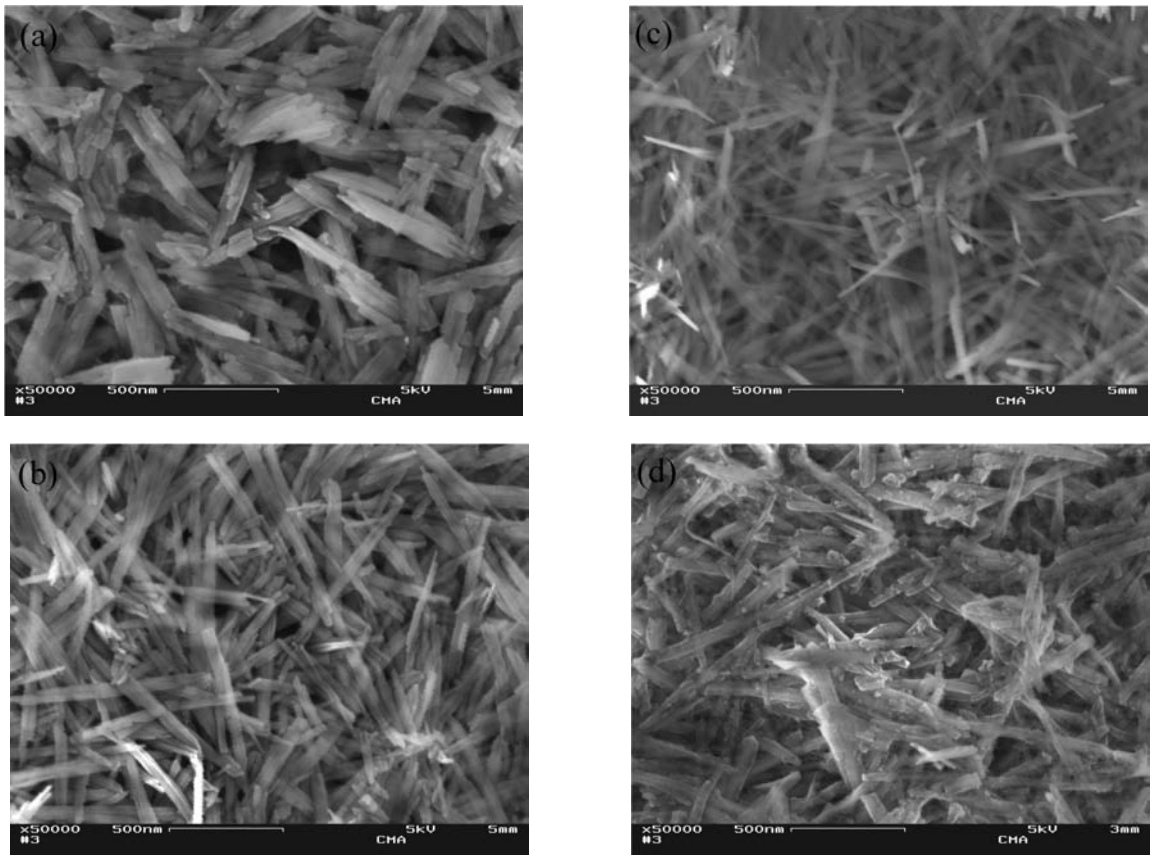


**FIGURE 1.** Changes in morphology with the Co content for samples (**a**) $G_3$, (**b**) $G_5$, (**c**) $G_7$, and (**d**) $G_{10}$ (50 000×).

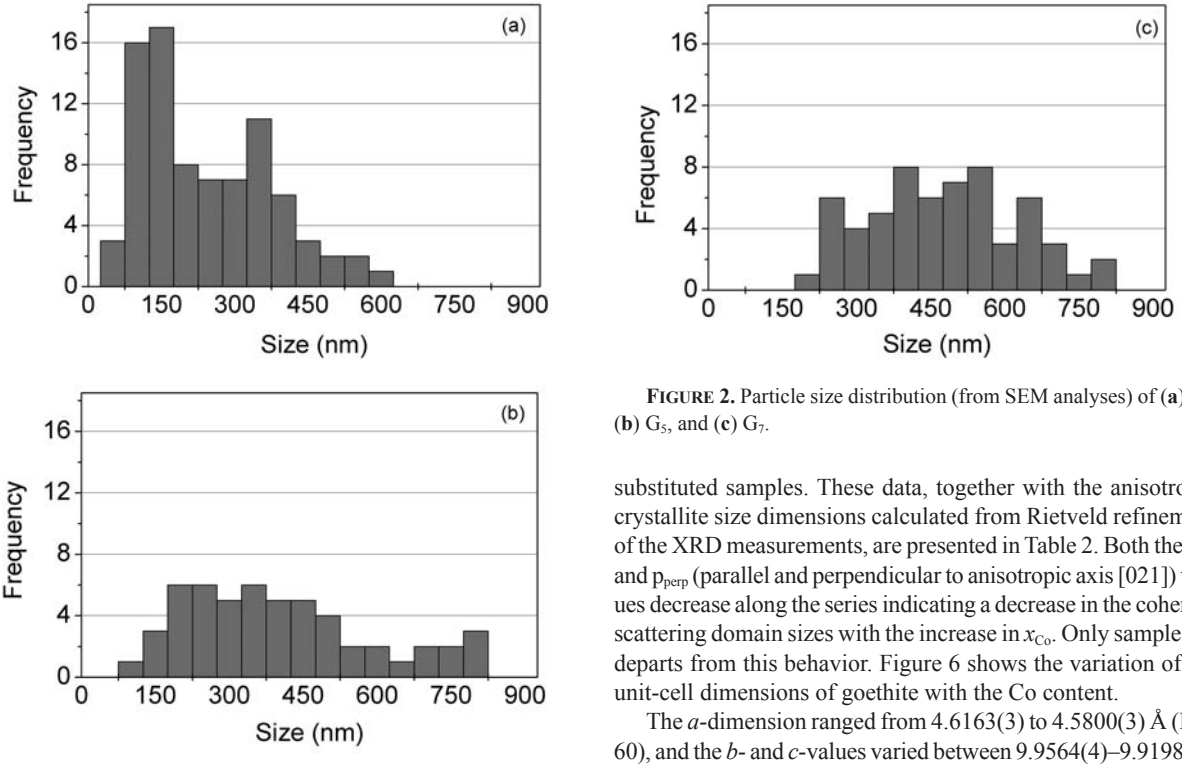


**FIGURE 2.** Particle size distribution (from SEM analyses) of (**a**) $G_3$, (**b**) $G_5$, and (**c**) $G_7$.

substituted samples. These data, together with the anisotropic crystallite size dimensions calculated from Rietveld refinement of the XRD measurements, are presented in Table 2. Both the $p_{par}$ and $p_{perp}$ (parallel and perpendicular to anisotropic axis [021]) values decrease along the series indicating a decrease in the coherent scattering domain sizes with the increase in $x_{Co}$. Only sample $G_{10}$ departs from this behavior. Figure 6 shows the variation of the unit-cell dimensions of goethite with the Co content.

The *a*-dimension ranged from 4.6163(3) to 4.5800(3) Å (Fig. 60), and the *b*- and *c*-values varied between 9.9564(4)–9.9198(4),

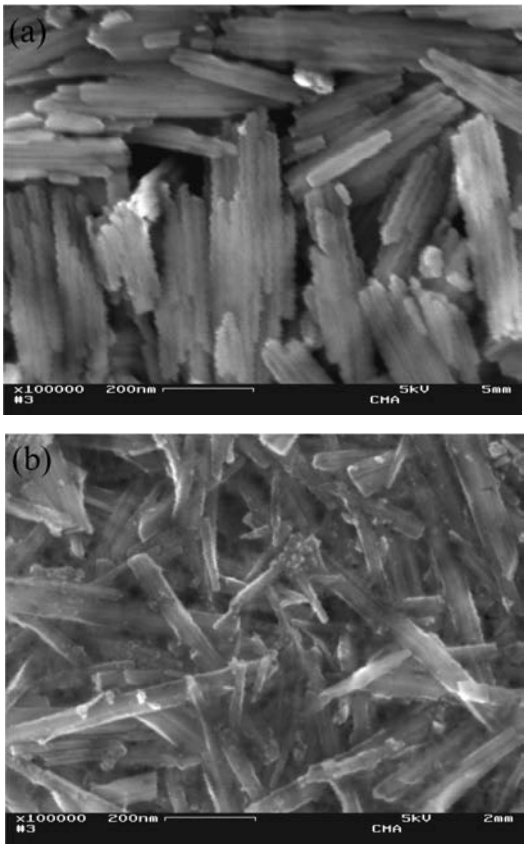


**FIGURE 3.** SEM images for samples (**a**) $G_0$ and (**b**) $G_{10}$ (magnification 100 000×).

**TABLE 2.** Lattice parameters and anisotropic crystallite dimensions

| Sample | *a* (Å) | *b* (Å) | *c* (Å) | *V* (Å³) | $p_{par}/p_{per}$ (Å) |
|---|---|---|---|---|---|
| $G_0$ | 4.6163(3) | 9.9564(4) | 3.0248(1) | 139.02(1) | 1234/193 |
| $G_3$ | 4.6070(3) | 9.9472(4) | 3.0210(1) | 138.44(1) | 1171/179 |
| $G_5$ | 4.5975(3) | 9.9395(4) | 3.0183(1) | 137.93(1) | 895/171 |
| $G_7$ | 4.5901(3) | 9.9309(4) | 3.0148(1) | 137.43(1) | 622/174 |
| $G_{10}$ | 4.5800(3) | 9.9198(4) | 3.0102(1) | 136.76(1) | 578/233 |

*Notes:* Numbers in parentheses are e.s.d. values for the least significant figures of the data shown; the values are taken from the final cycle of the Rietveld refinement.

and 3.0248(1)–3.0102(1) Å, respectively. Correspondingly, the unit-cell volume *V* ranged from 139.02(1) to 136.76(1) Å³. Good correlations ($0.997 \geq r^2 \geq 0.977$; n = 5) were obtained for linear regressions of all unit-cell parameters vs. $x_{Co}$. The calculated slopes were –0.00374, –0.00377, and –0.00150 Å/mol% Co for *a, b,* and *c,* respectively. A comparison with the slopes obtained by applying Vegard's rule [–0.0026, –0.0055, and –0.0018 for *a*, *b*, and *c* values calculated from JCPDS files 29-713 (goethite) and 26-480 (synthetic CoOOH with diaspore structure)] shows deviations from the predicted cell values, especially for the *a* parameter. The clear decrease in all unit-cell parameters with an increase in Co content indicates that $Co^{3+}$ rather than $Co^{2+}$ is incorporated in the goethite particles, since the ionic radii for $Co^{3+}$ cations in high-spin configuration (0.525 Å) is lower than that of high-spin $Fe^{3+}$ (0.65 Å) (Shannon and Prewitt 1969). This behavior is in agreement with the data reported by Gasser et al. (1996) for a series of Co-goethites synthesized in alkaline media.

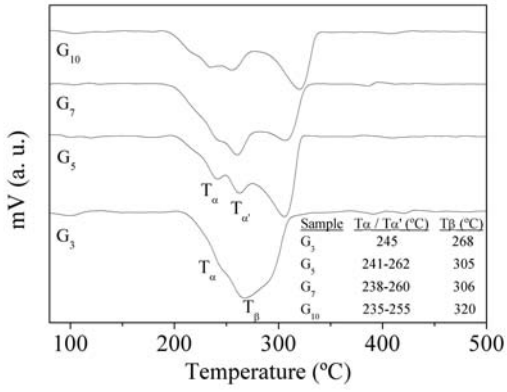


**FIGURE 4.** DTA traces of the particles formed with different values of Co/Fe.

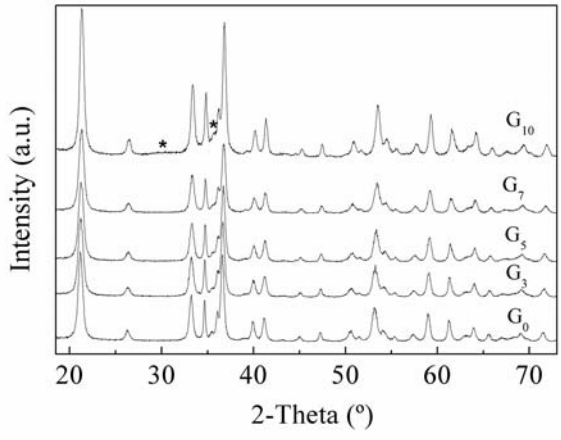


**FIGURE 5.** X-ray diffraction patterns of pure and Co-substituted goethites. * in sample $G_{10}$ indicate minor peaks at 30.2 and 35.7° corresponding to a separate phase.

The unit-cell parameter variations with the Co content are quite different from those observed for a series of Mn-goethites synthesized with a similar degree of substitution, although both $Mn^{2+}$ and $Co^{2+}$ were oxidized before incorporation into the goethite structure (Stiers and Schwertmann 1985; Cornell and Giovanoli 1989). This fact can be explained on the basis of the electronic configuration of $Mn^{3+}$, a $d^4$ ion that presents Jahn-Teller distortion of the octahedra, which generates an enlargement of the *b* parameter and a shortening of *a* and *c* parameters of the goethite.

Goethite crystallizes in the *Pbnm* space group. The cell contains four MeO(I)($O^{2+}$H) groups. The structure can be described as a hexagonal compact lattice made by the oxygen atoms O(I), corresponding to $O^{2-}$, and $O^{2+}$ atoms corresponding to $OH^-$ groups. The lattice is slightly distorted along (001). Half of the octahedral sites are filled with metal ions, but the others appear as vacancies (Fig. 7).

Due to the Rietveld refinement of atomic positions, the changes at the unit-cell level could be traced back to changes at the level of the fundamental octahedra. Structural results concerning pure goethite and Co-substituted goethites are compared in Table 3. Four kinds of distances between Me and O atoms are

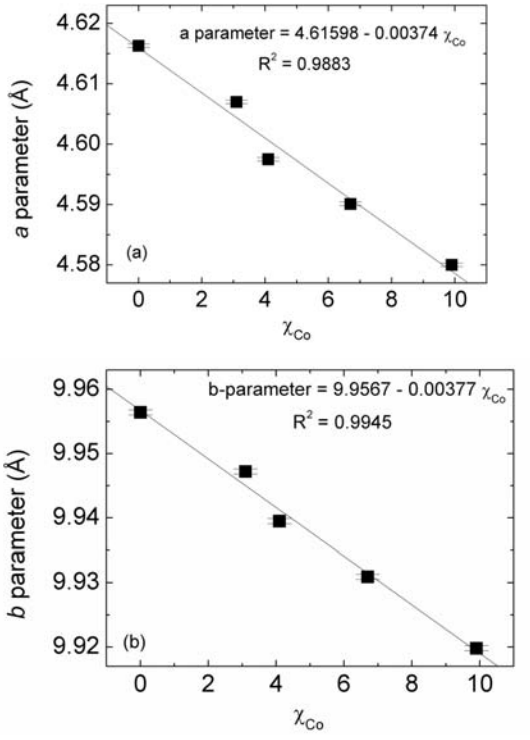


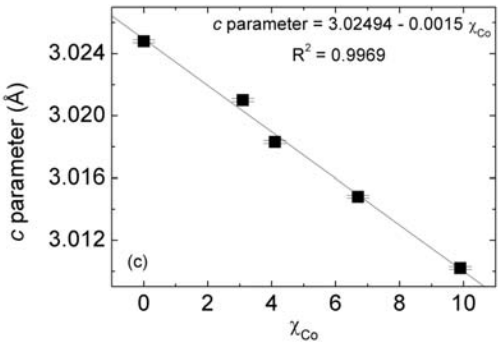


**FIGURE 6.** Unit-cell parameters vs. Co concentration.

**TABLE 3.** Results from the Rietveld refinement

| | $G_0$ | $G_3$ | $G_5$ | $G_7$ | $G_{10}$ |
|---|---|---|---|---|---|
| **Atom parameters** | | | | | |
| *x*(Me) | 0.0479(2) | 0.0473(2) | 0.0479(2) | 0.0474(2) | 0.0493(2) |
| *y*(Me) | −0.1459(1) | −0.1459(1) | −0.1454(1) | −0.1450(1) | −0.1449(1) |
| *x*[O(I)] | −0.2916(7) | −0.2862(6) | −0.2829(7) | −0.2941(7) | −0.2905(8) |
| *y*[O(I)] | 0.1982(3) | 0.1973(3) | 0.1982(3) | 0.1979(3) | 0.1975(4) |
| $x(O^{2+})$ | 0.1831(6) | 0.1889(6) | 0.1916(6) | 0.1898(6) | 0.1922(6) |
| $y(O^{2+})$ | 0.0529(3) | 0.0531(3) | 0.0534(3) | 0.0533(3) | 0.0530(4) |
| **Me-O distances** | | | | | |
| Me-$O_1$ | 1.951(2) | 1.970(4) | 1.947(4) | 1.948(4) | 1.962(2) |
| | 2 × 1.955(2) | 2 × 1.938(2) | 2 × 1.955(2) | 2 × 1.954(2) | 2 × 1.939(2) |
| Me-$O_2$ | 2.091(2) | 2.084(3) | 2.084(3) | 2.076(3) | 2.069(2) |
| | 2 × 2.094(2) | 2 × 2.078(2) | 2 × 2.080(2) | 2 × 2.069(2) | 2 × 2.079(2) |
| **Me-Me distances** | | | | | |
| E′ | 3.0248(1) | 3.0210(1) | 3.0183(1) | 3.0148(1) | 3.0102(1) |
| E | 3.306(1) | 3.300(2) | 3.291(2) | 3.280(2) | 3.276(1) |
| DC | 3.451(1) | 3.447(1) | 3.447(1) | 3.447(1) | 3.444(1) |
| **Agreement factors for the refinements** | | | | | |
| $R_{wp}$ | 9.93 | 9.97 | 10.11 | 10.20 | 9.13 |
| $R_p$ | 7.45 | 7.51 | 7.51 | 7.73 | 6.81 |
| $R_B$ | 3.98 | 3.67 | 3.68 | 4.68 | 6.73 |
| GofF* | 1.17 | 1.14 | 1.16 | 1.16 | 1.47 |

*Notes:* $R_p = 100\Sigma|I_o - I_c|/\Sigma I_o$; $R_{wp} = 100[\Sigma w_i(I_o - I_c)^2/\Sigma w_i I_o^2]^{0.5}$. $R_B = 100\Sigma|I_{ko} - I_{kc}|/\Sigma I_{ko}$; GofF = $\Sigma w_i(I_o - I_c)^2/(n - p)$. $I_o$ and $I_c$ = observed and calculated intensities. $w_i$ = weight assigned to each step intensity. $I_{ko}$ and $I_{kc}$ = observed and calculated intensities for Bragg k-reflection. n and p = number of data points in the pattern and number of parameters refined. Goethite = Space group *Pbnm*, z-coordinates of all atoms are 0.25. Interatomic distances calculated using the DISAGL subroutine in the GSAS system.
*GofF = Goodness of Fit.

observed [for $G_{10}$ sample, Me-O(I): 1.962(2) and 1.939(2) Å; Me-$O^{2+}$: 2.069(2) and 2.079(2) Å]. The difference in the Fe-O(I) and Fe-$O^{2+}$ distances in $G_0$ (pure goethite) are small and may be described by only two distances [Fe-O(I): 1.951 and 1.955 Å; Me-$O^{2+}$: 2.091 and 2.094 Å (estimated errors are ±0.002 Å in all cases)]. So, average Me-O(I), Me-$O^{2+}$ distances decrease with the Co content revealing an average smaller coordination polyhedron around the metal ion (Table 3). Statistical metal-metal distances also decrease with increasing $x_{Co}$. However, they decrease in a different fashion: the decrease of the E′ distance is stronger than that of E, and the DC distance shows the least variation.

### Dissolution behavior

Figure 8 illustrates the amount of dissolved Fe vs. time for the samples. The lines show a curvilinear relation. However, for samples $G_0$ to $G_7$ and time values ≤330 min, the traces can be fitted with a linear relation (correlation coefficients: $0.999 \geq R^2 \geq 0.990$, $n = 7$ for each sample).

Initial dissolution rates ranged from 0.0111 to 0.0312 µmol Fe/g oxide·min and increased with increasing Co concentration. $G_{10}$ sample displays an initial dissolution rate of 0.0595 µmol Fe/g oxide·min, and the kinetic profile shows a higher value of Fe being dissolved at the beginning of the dissolution. This fact may be due to a small proportion of amorphous Fe or Fe-oxides crystals of small size, which is in line with the increment of the surface area of this sample (Table 1). Values of the initial rates are presented in Table 4.

The same trend is observed when rate data are expressed in terms of µmol Fe/$m^2$ min, with values ranging from 0.285 to 0.580 going from $G_0$ to $G_{10}$.

### Congruency of dissolution of Co and Fe

Plots of the fraction of Co vs. the fraction of Fe dissolved during dissolution provide an indirect measure of the distribution of Co within the crystals of goethite. Dissolution data for Fe and Co (sample $G_5$) are shown in Figure 9. The data for $G_5$ are well described by a line of slope ≈1, that is, the ratio Co/Fe remained almost unaffected by the duration of the experiment, strongly suggesting that $Co^{3+}$ and $Fe^{3+}$ are uniformly distributed within the crystal structure of goethite, resulting in a nearly congruent dissolution of the Co-goethites.

### Effect of dissolution temperature—activation energy

The activation energy ($E_a$) for the dissolution process was obtained for samples $G_0$ and $G_7$ using the Arrhenius equation, with $R^2$ values ≥ 0.98. The dissolution rate ($k$) values were obtained from the slopes of initial nearly linear regions of the dissolution curves measured at 40, 50, and 60 °C (Fig. 10). The calculated $E_a$ values are 147.4 kJ/mol for pure goethite and 78.2 kJ/mol for Co-substituted goethite ($G_7$). The smaller value in $G_7$ may

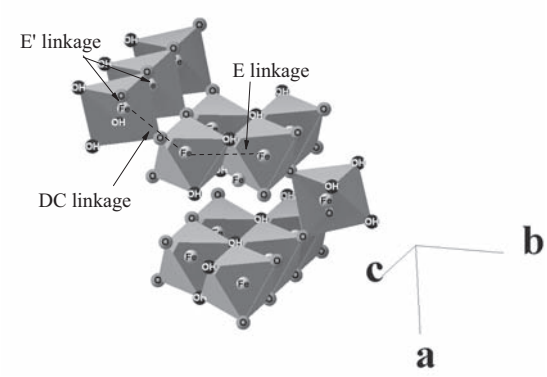


**FIGURE 7.** Arrangement of polyhedra in the structure of goethite, the octahedra share edges within the rows, and vertices between chains.

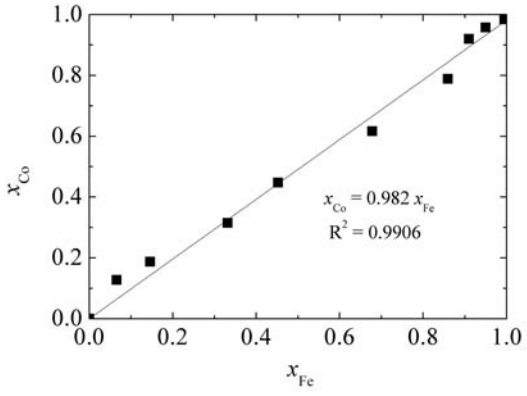


**FIGURE 9.** Plot of $x_{Co}$ vs. $x_{Fe}$ dissolved in 4 *M* HCl for sample $G_5$.

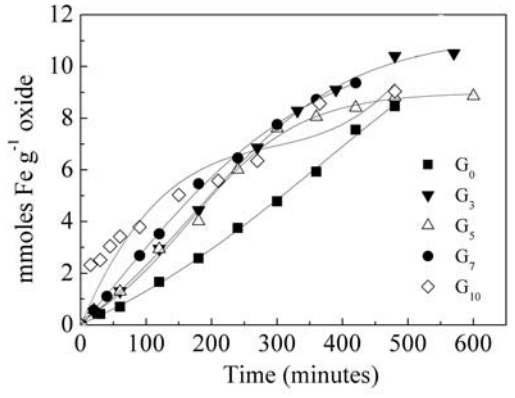


**FIGURE 8.** Representative dissolution curves for synthetic goethites in 4 mol/dm$^3$ HCl at 40 °C vs. time, as affected by Co substitution

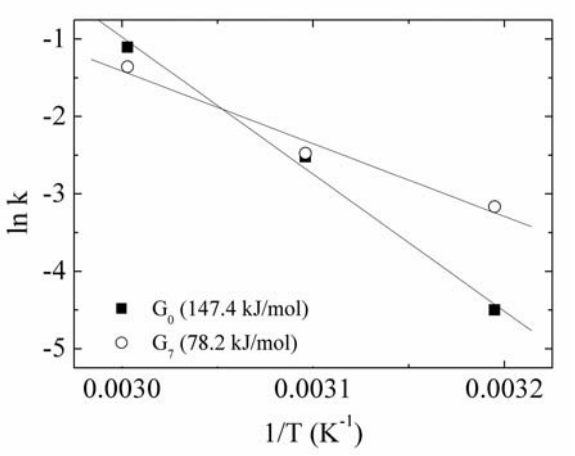


**FIGURE 10.** Activation energy determination from the Arrhenius equation in its linear form for $G_0$ and $G_7$ samples.

be ascribed to the presence of weaker $Co^{3+}$-O bonds compared to the only $Fe^{3+}$-O bonds present in pure goethite.

The comparison between pure goethite, Co-goethite, and Mn-goethite ($E_a$ = 90.1 kJ/mol) with a similar degree of substitution obtained by a similar synthesis (Alvarez et al. 2006) displays the following order in the reactivity in acid media:

Co-goethite > Mn-goethite > goethite

Coefficients obtained from data fitted to the Kabai equation in its linear form

$$\ln\ln\left[\frac{1}{1-x_{Fe}}\right] = \alpha \ln k + \alpha \ln t$$

for samples dissolved at 40 °C are listed in Table 5.

The dissolution rate constant, *k*, increased as Co substitution increased. For sample $G_{10}$, two intercepting straight lines were required to achieve a better fit. This behavior could be attributed to the coexistence of an additional phase together with goethite; the decrease of its rate constant calculated from the linear region I (attributed to the goethite dissolution) respect to the other samples may be due to a smaller Co content in the goethite phase.

The combined effects of surface area and Co substitution are responsible for the increase of the dissolution rate constant (k). Substitution Co in goethite reduces crystal size and therefore increases the surface area, and acid attack destroys the Co-O bond more quickly than the Fe-O bond.

**TABLE 4.** Initial dissolution rate for goethites as affected by Co

| Sample | Initial rate (mmoles Fe/g oxide min) | $R^2$ | n |
|---|---|---|---|
| $G_0$ | 0.0111 | 0.998 | 11 |
| $G_3$ | 0.0217 | 0.999 | 10 |
| $G_5$ | 0.0246 | 0.993 | 11 |
| $G_7$ | 0.0312 | 0.999 | 10 |
| $G_{10}$ | 0.0595 | 0.918 | 11 |

**TABLE 5.** Dissolution rate constant for dissolution–time profiles fitted to the Kabai equation

| Sample | k × 10$^{-3}$/min | $R^2$ | *n* | Linear part |
|---|---|---|---|---|
| $G_0$ | 2.268 | 0.991 | 9 | I |
| $G_3$ | 3.417 | 0.993 | 9 | I |
| $G_5$ | 3.499 | 0.991 | 10 | I |
| $G_7$ | 5.218 | 0.992 | 9 | I |
| $G_{10}$ | 3.411 | 0.978 | 7 | I |
| | 4.098 | 0.982 | 3 | II |

## ACKNOWLEDGMENTS

The authors acknowledge María Rosa Prat for her special collaboration in the DTA measurements. This research was partially supported by grant from UBACYT X800, PICT 32469 (2005) and by Secretaría de Ciencia y Tecnología (UNS).

## REFERENCES CITED


Alloway, B.J. (1990) Heavy Metals in Soils, 339 p. Blackie Academic and Professional, Glasgow.

Alvarez, M., Rueda, E.H., and Sileo, E.E. (2006) Structural characterization and chemical reactivity of synthetic Mn-goethites and hematites. Chemical Geology, 231, 288–299.

——— (2007) Simultaneous incorporation of Mn and Al in the goethite structure. Geochimica et Cosmochimica Acta, 71, 1009–1020.

Cornell, R.M. (1991) Simultaneous incorporation of Mn, Ni, and Co in the goethite (α-FeOOH) structure. Clay Minerals, 2, 427–430.

Cornell, R.M. and Giovanoli, R. (1989) Effect of cobalt on the formation of crystalline iron oxides from ferrihydrite in alkaline media. Clays and Clay Minerals, 37, 65–70.

Cornell, R.M. and Schwertmann, U. (1996) The Iron Oxides: Structure, Properties, Reactions, Occurrence and Uses, 573 p. VCH, Weinheim (Federal Republic of Germany).

Cornell, R.M., Posner, A.M., and Quirk, J.P. (1974) Crystal morphology and the dissolution of goethite (α-FeOOH). Journal of Inorganic and Nuclear Chemistry, 36, 1937–1946.

Finger, L.W., Cox, D.E., and Jephcoat, A.P. (1994) A correction for powder diffraction peak asymmetry due to axial divergence. Journal of Applied Crystallography, 27, 892–900

Gasser, U.G., Jeanroy, E., Mustin, C., Barres, O., Nuesch, R., Bethelin, J., and Herbillon, A.J. (1996) Properties of synthetic goethites with Co for Fe substitution. Clay Minerals, 31, 465–476.

Gerth, J. (1990) Unit cell dimensions of pure and trace metal-associated goethites. Geochimica et Cosmochimica Acta, 54, 363–371.

Ishikawa, T., Yamashita, H., Yasukawa, A., Kandori, K., Nakayama, T., and Yuse, F. (2000) Structures of Ti(IV)-doped α-FeOOH particles. Journal of Materials Chemistry, 10, 543–57.

Iwasaki, K. and Yamamura, T. (2002) Whisker-like goethite nanoparticles containing cobalt synthesized in a wet process. Materials Transactions, 43, 2097–2103.

Kühnel, R.A., Roorda, H.J., and Steensma, J.J. (1975) The crystallinity of minerals. A new variable in pedogenic processes: A study of goethite and associated silicates in laterites. Clays and Clay Minerals, 23, 349–354.

Larson, A.C. and Von Dreele, R.B. (2004) General Structure Analysis System (GSAS). Los Alamos National Laboratory Report LAUR 86–748.

Lim-Nuñez, R.S.L. and Gilkes, R.J. (1987) Acid dissolution of synthetic metal-containing goethite and hematite. Proceedings of the International Clay Conference, Denver, p. 197–204.

Murad, E. and Schwertmann, U. (1983) The influence of aluminum substitution and crystallinity on the Mössbauer spectra of goethite. Clay Minerals, 18, 301–312.

Norrish, K. (1975) Geochemistry and mineralogy of trace elements. In A.R. Nicholas and D.J. Egan, Eds., Trace Elements in Soil-Plant-Animal System, p. 55–81. Academic Press, New York.

Nuñez, N.O., Tartaj, P., Morales, M.P., Pozas, R., Ocaña, M., and Serna, C.J. (2003) Preparation, characterization and magnetic properties of Fe-based alloy particles with elongated morphology. Chemistry of Materials, 15, 3558–3563.

Pozas, R., Ocaña, M., Morales, M.P., and Serna, C.J. (2002) Uniform nanosized goethite particles obtained by aerial oxidation in the $FeSO_4$-$Na_2CO_3$ system. Journal of Colloid and Interface Science, 254, 87–94.

Pozas, R., Rojas, T.C., Ocaña, M., and Serna, C.J. (2004) The nature of Co in synthetic Co-substituted goethites. Clays and Clay Minerals, 52, 760–766.

Rietveld, H.M. (1969) A profile refinement method for nuclear and magnetic structures. Journal of Applied Crystallography, 2, 65–71.

Schulze, D.G. and Schwertmann, U. (1984) The influence of aluminum on iron oxides. X. Properties of Al-substituted goethites. Clay Minerals, 19, 521–539.

Schwertmann, U. (1984) The influence of aluminum on iron oxides. IX. Dissolution of Al-goethites in 6 *M* HCl. Clay Minerals, 22, 83–92.

Schwertmann, U. and Taylor, R.M. (1989) Iron oxides. In J.B Dixon and S.B. Weed, Eds., Minerals in Soil Environments, p. 380–438. Soil Science Society of America, Madison, Wisconsin.

Shannon, R.D. and Prewitt, C.T. (1969) Effective ionic radii in oxides and fluorides. Acta Crystallographica, B25, 925–946.

Sidhu, P.S., Gilkes, R.J., Cornell, R.M., and Posner, A.M. (1981) Dissolution of iron oxides and oxyhydroxides in hydrochloric and perchloric acids. Clays and Clay Minerals, 29, 269–276.

Sileo, E.E., Alvarez, M., and Rueda, E.H. (2001) Structural studies on the manganese for iron substitution in the synthetic goethite-jacobsite system. The International Journal of Inorganic Materials, 3, 271–279.

Sileo, E.E., Ramos, A.Y., Magaz, G.E., and Blesa, M.A. (2004) Long-range vs. Short-range ordering in synthetic Cr-substituted goethites. Geochimica et Cosmochimica Acta, 68, 3053–3063.

Stephens, P.W. (1999) Phenomenological model of anisotropic broadening in powder diffraction. Journal of Applied Crystallography, 32, 281–289.

Stiers, W. and Schwertmann, U. (1985) Evidence for manganese substitution in synthetic goethite. Geochimica et Cosmochimica Acta, 49, 1909–1911.

Sun, X., Doner, H.E., and Zavarin, M. (1999) Spectroscopy study of arsenite [As(III)] oxidation on Mn-substituted goethite. Clays and Clay Minerals, 4, 474–480.

Szytula, A., Burewicz, A., Dimitrijevic, Z., Krasnicki, S., Rzany, H., Todorovic, J., Wanic, A., and Wolski, W. (1968) Neutron diffraction studies of α-FeOOH. Physica Status Solidi, 26, 429–434.

Thompson, P., Cox, D.E., and Hastings, J.B. (1987) Rietveld refinement of Debye-Scherrer synchrotron X-ray data from $Al_2O_3$. Journal of Applied Crystallography, 20, 79–83.

Wolska, E. and Schwertmann, U. (1989) Nonstoichiometric structures during dehydroxylation of goethite. Zeitschrift für Kristallographie, 189, 223–237.



MANUSCRIPT RECEIVED FEBRUARY 15, 2007
MANUSCRIPT ACCEPTED OCTOBER 1, 2007
MANUSCRIPT HANDLED BY RICHARD WILKIN